Change in energy eigenvalues against parameters

Toshihiro Iwai and Boris Zhilinskii

Abstract. A topological characterization of energy-band rearrangements against parameters for molecular problems with slow/fast variables comes around to a study of a Dirac equation with a parameter. In this article, the Dirac equation of space-dimension two is studied under both the APS (an abbreviation of Atiyah-Patodi-Singer) and the chiral bag boundary conditions, where the mass is viewed as a parameter ranging over all real numbers. The APS boundary condition requires that eigenstates evaluated on the boundary should belong to the subspace of eigenstates associated with positive or negative eigenvalues for a boundary operator, and the chiral bag boundary condition requires that eigenstates evaluated on the boundary have chiral components related by a unitary operator. The spectral flow for a one-parameter family of operators is the net number of eigenvalues passing through zeros in the positive direction as the parameter runs. It is shown that the spectral flow for the Dirac equation with the APS boundary condition is ± 1, depending on the sign of the total angular momentum eigenvalue. A counterpart of the spectral flow in the case of the chiral bag boundary condition is treated as an extension of spectral flow. In addition, discrete symmetry is discussed to explain the pattern of eigenvalues as functions of the parameter.

1. Setting up

There is a class of band structures of molecular spectra, in which energy excitations can be separated into low and high ones. For example, the energy of typical rotational excitation is much smaller than the typical vibrational excitation (see Fig. 1). The low and the high excited levels form high density states and a small number of isolated states, respectively. Accordingly, the

whole dynamical variables are separated into slow and fast variables in such a way that the slow variables are for describing high density states and the fast ones for a small number of isolated states.
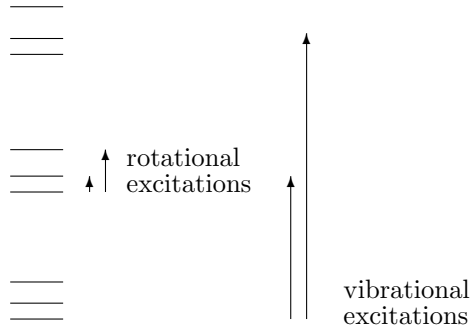

FIGURE 1. A characteristic pattern of energy levels for a molecular problem with one slow (rotational) and one fast (vibrational) degrees of freedom.

We give a simple model Hamiltonian consisting of slow and fast variables of different nature. Let J_k and S_k be generators of $SU(2)$, which are taken as describing the orbital and the spin variables, respectively. We define a one-parameter family of Hamiltonian operators to be

$$\hat{H}_\tau = (1 - \tau)\mathbb{1} \otimes (-S_3) + \tau \sum_{k=1}^{3} J_k \otimes S_k, \quad 0 \leq \tau \leq 1. \tag{1}$$

For the representation parameters $j = 1, s = \frac{1}{2}$, the $\hat{H}_\tau$ takes the form of 6×6 Hermitian matrix. The eigenvalues are easily found as functions of the parameter τ, which exhibit the band rearrangement against τ, as is shown in Fig. 2.

If j is sufficiently large, the J_k can be taken as slow variables and treated as classical ones but the fast variables S_k remain to be quantum ones. The treatment of slow and fast variables as classical and quantum variables, respectively, is called a semi-quantum model.

On the assumption that the J_k can be treated as classical variables [2], the operator $\hat{H}_\tau$ with J_k replaced by x_k is converted into

$$H_\tau(\boldsymbol{x}) = \frac{1 - \tau}{2} \begin{pmatrix} -1 & 0 \\ 0 & 1 \end{pmatrix} + \frac{\tau}{2} \begin{pmatrix} x_3 & x_1 - ix_2 \\ x_1 + ix_2 & -x_3 \end{pmatrix}, \quad \boldsymbol{x} \in S^2 \subset \mathbb{R}^3, \tag{2}$$

where $\boldsymbol{x} = (x_k)$ has been restricted to the unit sphere S^2 by the normalization J_k/J due to the conservation of the angular momentum. The eigenvalues of $H_\tau(\boldsymbol{x})$ are

$$\lambda^\pm(\tau, \boldsymbol{x}) = \pm\sqrt{-\frac{1}{4} + \frac{\tau(1 - \tau)}{2}(1 + x_3)}, \quad |\boldsymbol{x}| = 1, \tag{3}$$

The legend in the figure reads:

-τ/4+sqrt(0.25-(3*τ)/4+(17*τ**2)/16) ———
-τ/4-sqrt(0.25-(3*τ)/4+(17*τ**2)/16) ------
-τ/4+sqrt(0.25-τ/4+(9*τ**2)/16) ········
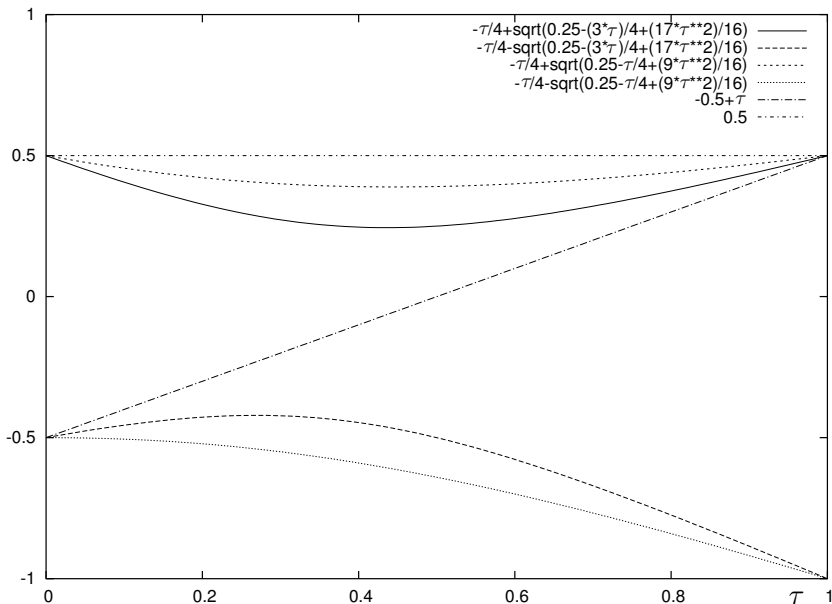-τ/4-sqrt(0.25-τ/4+(9*τ**2)/16) ········
-0.5+τ —·—·—
0.5 —··—··

FIGURE 2. A redistribution of eigenvalues for $\hat{H}_\tau$ against the parameter τ.

which are degenerate if and only if $x_3 = 1$ (or $\boldsymbol{x} = \boldsymbol{e}_3 = (0,0,1)$) and $\tau = \frac{1}{2}$.

For each of eigenvalues $\lambda^\pm(\tau, \boldsymbol{x})$, the associated eigenspace is attached at $\boldsymbol{x} \in S^2$, and the totality of such eignspaces forms a complex line bundle over S^2, which we denote by $L^\pm(\tau)$, respectively, and call the eigen-line bundles. As long as the eigenvalues are not degenerate, we have the direct sum of eigen-line bundles, $L^+(\tau) \oplus L^-(\tau)$. When $\tau = 0$, both of the eigen-line bundles are trivial; $L^\pm(0) = S^2 \times \mathbb{C}$. When the parameter passes the value $\tau = \frac{1}{2}$, the direct sum of the eigen-line bundles fails, since the eigenvalues are degenerate at $\boldsymbol{x} = \boldsymbol{e}_3$ for $\tau = \frac{1}{2}$. This means that accompanying the variation in the parameter τ, the eigen-line bundles topologically change. This change can be detected by using the first Chern number assigned to each of $L^\pm(\tau)$. For $\tau = 1$, the Hamiltonian is expressed as

$$H_1(\boldsymbol{x}) = \frac{1}{2} \begin{pmatrix} x_3 & x_1 - ix_2 \\ x_1 + ix_2 & -x_3 \end{pmatrix}, \quad \boldsymbol{x} \in S^2 \subset \mathbb{R}^3, \tag{4}$$

and the first Chern numbers of $L^\pm(1)$ are easily calculated as

$$c_1(L^\pm(1)) = \frac{i}{2\pi} \int_{S^2} F^\pm = \mp 1, \tag{5}$$

where $F^\pm$ denote the curvature forms assigned to $L^\pm(1)$, respectively. Since the Chern number is integer-valued and depends continuously on the parameter τ, it is constant in τ except for $\tau = \frac{1}{2}$. Thus, the modification of band

structure against the parameter τ shown in Fig. 2 finds a counterpart in the corresponding semi-quantum model, in the form of a piece-wise constant behavior of Chern numbers shown in Fig. 3.
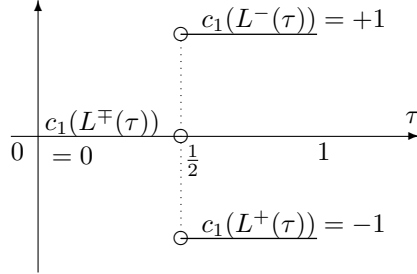

FIGURE 3. Change in the Chern numbers against τ for the semi-quantum model (2).

We give here, after [3], a more complicated semi-quantum Hamiltonian than (2),

$$H(\boldsymbol{x}) = \begin{pmatrix} X & Y - iZ \\ Y + iZ & -X \end{pmatrix}, \quad \boldsymbol{x} \in S^2 \subset \mathbb{R}^3, \tag{6}$$

where

$$X(\boldsymbol{x}) = b_1(y^2 - x^2) + b_2 zy, \tag{7a}$$

$$Y(\boldsymbol{x}) = 2b_1 yx - b_2 zx, \tag{7b}$$

$$Z(\boldsymbol{x}) = a_1 z + a_2 y(y^2 - 3x^2), \tag{7c}$$

and (a_1, a_2, b_1, b_2) are real constants with the assumption that $(a_1, a_2) \neq (0, 0)$ and $(b_1, b_2) \neq (0, 0)$. We note that this Hamiltonian admits D_3 symmetry,

$$D^E(g)H(\boldsymbol{x})D^E(g)^{-1} = H(D^{E \oplus A_2}(g)\boldsymbol{x}), \quad g \in D_3, \tag{8}$$

where D_3 is a discrete subgroup of $SO(3)$ and where E and A_2 denote a two-dimensional and one-dimensional not totally-symmetric representations of D_3, respectively. The action of D_3 on the sphere, denoted by the symbol $D^{E \oplus A_2}$, is illustrated in Fig. 4. The z axis is the C_3 symmetry axis. Three C_2 symmetry axes belong to the xy plane. Two intersection points of the C_3 symmetry axis and the sphere form the two-point orbit with C_3 stabilizer. Six points of intersection of three C_2 symmetry axes with the sphere form two three-point orbits with stabilizer C_2.

After [3], we describe the Chern numbers of the eigen-line bundles for the Hamiltonian (6). Owing to the invariance of the Chern numbers with respect to the scaling of the parameters (a_1, a_2, b_1, b_2), the parameter space $(\mathbb{R}^2 - \{0\}) \times (\mathbb{R}^2 - \{0\})$ reduces to the two-torus T^2 described as $a_1 = \cos\phi_1, a_2 = \sin\phi_1$ and $b_1 = \cos\phi_2, b_2 = \sin\phi_2$. The reduced parameter space is divided into a certain number of connected regions to which respective fixed Chern numbers are assigned, and such regions are called iso-Chern domains. The
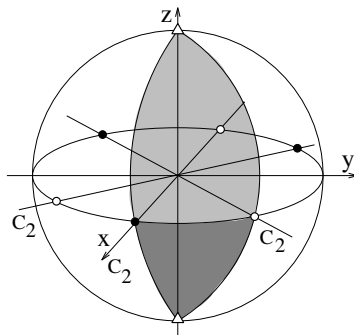
FIGURE 4. D_3 group and its action on the sphere.

parameter space with such partition and Chern numbers is called the iso-Chern diagram. The iso-Chern diagram for the eigen-line bundle associated with the positive eigenvalue is shown in Fig. 5. The red and blue lines ($\phi_1 = \pm\frac{\pi}{2}, \phi_2 = \pm\frac{\pi}{2}$) and black curves ($\cos\phi_1 \cos\phi_2 = \sin\phi_1 \sin^3\phi_2$) are the sets of degeneracy points in the reduced parameter space T^2.

The iso-Chern diagram for the eigen-line bundle associated with negative eigenvalue is obtained by opposing the sign of the Chern number assigned to each iso-Chern domain.
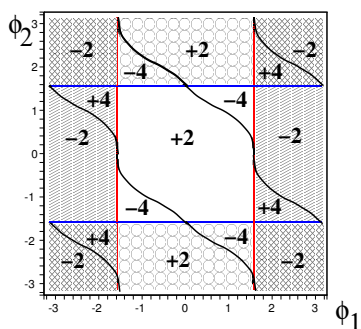

FIGURE 5. The iso-Chern diagram for the eigen-line bundle associated with the positive eigenvalue of the D_3 invariant Hamiltonian (6)

In view of Fig. 5, we observe that when we move from an iso-Chern domain to an adjacent one, passing the boundary between them, the change in the Chern number, which we call a delta-Chern, is one of the four values, $\pm 2, \pm 6$. The numbers 2 and 6 are those of D_3 orbits with stabilizers C_3 and C_2, respectively. In fact, we can show that degeneracy points on S^2 form D_3 orbits and that the delta-Chern is given by "± 1 times the order of the orbit in question". The number $+1$ or -1 originally comes from a winding number,

and is called a local delta-Chern, which has already appeared in Fig. 3. In the case of Hamiltonian (2), the number of degeneracy points is one and the initial bundle $L^{\pm}(\tau)$ with $\tau < \frac{1}{2}$ is trivial, so that the delta-Chern and the local delta-Chern coincide.

The local delta-Chern can be evaluated through a linearization method at the degeneracy point in question. Let $(\tau_0, \boldsymbol{x}_0)$ be a degeneracy point, where τ_0 is a parameter value at which a path in the parameter space crosses the boundary between adjacent iso-Chern domains and where $\boldsymbol{x}_0$ is a degeneracy point on the sphere at which the two eigenvalues are degenerate for τ_0. Then, the Hamiltonian can be homotopically deformed to the linearized Hamiltonian $H_{\mathrm{loc}}(t, p; \tau_0, \boldsymbol{x}_0)$ in the neighborhood of $(\tau_0, \boldsymbol{x}_0)$ by means of deleting higher order terms in (t, p_1, p_2), and hence the winding number attached to the degeneracy point can be evaluated by using $H_{\mathrm{loc}}(t, p; \tau_0, \boldsymbol{x}_0)$ to obtain the local delta-Chern. This idea is mentioned not in [3] but in [6]. For the semi-quantum Hamiltonian (2), the linearized Hamiltonian at $(\tau, \boldsymbol{x}) = (\frac{1}{2}, \boldsymbol{x}_0)$ is given by

$$H_{\mathrm{loc}}(t, q; \frac{1}{2}, \boldsymbol{x}_0) = t\dot{H}_{\frac{1}{2}}(\boldsymbol{x}_0) + p_1 \nabla H_{\frac{1}{2}}(\boldsymbol{x}_0) \cdot \boldsymbol{e}_1 + p_2 \nabla H_{\frac{1}{2}}(\boldsymbol{x}_0) \cdot \boldsymbol{e}_2$$
$$= \frac{1}{4} \begin{pmatrix} 4t & p_1 - ip_2 \\ p_1 + ip_2 & -4t \end{pmatrix}, \quad (9)$$

where $\boldsymbol{e}_k$ are the standard basis vectors with $\boldsymbol{x}_0 = \boldsymbol{e}_3$, and where $\boldsymbol{e}_1, \boldsymbol{e}_2$ are viewed as tangent vectors to S^2 at $\boldsymbol{x}_0$.

We are interested in what corresponds to the delta-Chern, in full quantum description. To this end, we consider a full quantum Hamiltonian corresponding to a linearized semi-quantum Hamiltonian. For notational simplicity, we take up the simple semi-quantum Hamiltonian, in place of (9),

$$H(t, p) = \begin{pmatrix} t & p_1 - ip_2 \\ p_1 + ip_2 & -t \end{pmatrix}. \quad (10)$$

Replacing p_k by $-i\partial/\partial q_k$, we obtain the corresponding full quantum Hamiltonian expressed as

$$\hat{H}_t = \begin{pmatrix} t & -i\frac{\partial}{\partial q_1} - \frac{\partial}{\partial q_2} \\ -i\frac{\partial}{\partial q_1} + \frac{\partial}{\partial q_2} & -t \end{pmatrix} = -i\sum_{k=1}^{2} \sigma_k \frac{\partial}{\partial q_k} + t\sigma_3, \quad (11)$$

where σ_k are the Pauli matrices. Thus we come to a Dirac operator $\hat{H}_t$.

2. The Dirac equation on a bounded domain

A Dirac operator on $\mathbb{R}^d$ is given by

$$H = -i\sum_{k=1}^{d} \gamma_k \nabla_k + \mu\gamma_{d+1}, \quad \nabla_k = \partial/\partial x_k, \quad (12)$$

where μ is a mass parameter which is assumed to take all real values in this article, and where γ_k are the gamma matrices satisfying

$$\gamma_k \gamma_j + \gamma_j \gamma_k = 2\delta_{jk} I, \quad j, k = 1, \ldots, d,$$
$$\gamma_k \gamma_{d+1} + \gamma_{d+1} \gamma_k = 0,$$
$$(\gamma_{d+1})^2 = I,$$
$$(\gamma_\nu)^\dagger = \gamma_\nu, \quad \nu = 1, \ldots, d, d+1,$$

with I denoting the $d \times d$ identity matrix. In the present article, our interest centers on the case of $d = 2$, and the gamma matrices are realized as the Pauli matrices, $\gamma_\nu = \sigma_\nu$, $\nu = 1, 2, 3$ (see (11)).

To pose a boundary condition, we need Green's formula [1]. Let V and S denote a bounded domain in $\mathbb{R}^d$ and its boundary, respectively. Green's formula for the Dirac operator H is given by

$$\langle \Phi, H\Psi \rangle_V - \langle H\Phi, \Psi \rangle_V = -i\langle \phi, \vec{\gamma} \cdot \vec{n}\, \psi \rangle_S, \tag{13}$$

where $\phi = \Phi|_S, \psi = \Psi|_S$ and $\vec{\gamma} \cdot \vec{n} = \sum \gamma_j n_j$ with $\vec{n}$ being the outward unit normal to S.

Any boundary condition for the Dirac equation $H\Phi = E\Phi$ should require the vanishing of the right-hand side of the above equation. If such a boundary condition is adopted, the operator H becomes a symmetric operator. Furthermore, with some Sobolev conditions, it becomes self-adjoint.

In what follows, we give two boundary conditions, the APS and the chiral bag boundary conditions. The APS boundary condition is given as follows: If we can find a self-adjoint boundary operator B on S such that B has no zero eigenvalue, we obtain the decomposition of the Hilbert space $\mathcal{H}(S)$ into

$$\mathcal{H}(S) = \mathcal{H}^{(+)}(S) \oplus \mathcal{H}^{(-)}(S), \tag{14}$$

where $\mathcal{H}^{(\pm)}(S)$ are subspaces such that $B|_{\mathcal{H}^{(+)}(S)} > 0$ and $B|_{\mathcal{H}^{(-)}(S)} < 0$. We assume further that

$$(\vec{\gamma} \cdot \vec{n})\mathcal{H}^{(\pm)}(S) = \mathcal{H}^{(\mp)}(S). \tag{15}$$

The APS boundary condition requires that eigenstates evaluated on the boundary should belong to $\mathcal{H}^{(+)}(S)$ or $\mathcal{H}^{(-)}(S)$.

To describe the chiral bag boundary condition, we decompose spinors into the sum of chiral components,

$$\Phi = \Phi_+ + \Phi_-, \quad \Phi_\pm := \frac{1}{2}(I \pm \vec{\gamma} \cdot \vec{n})\Phi. \tag{16}$$

The components $\Phi_\pm$ belong to the eigenspaces associated with the eigenvalues ± 1 of $\vec{\gamma} \cdot \vec{n}$, respectively, and those eigenspaces are orthogonal to each other, so that any chiral components, $\Phi_\pm$ and $\Psi_\pm$, satisfy

$$\vec{\gamma} \cdot \vec{n}\, \Phi_+ = \Phi_+, \quad \vec{\gamma} \cdot \vec{n}\, \Phi_- = -\Phi_-, \quad \langle \Psi_+, \Phi_- \rangle = 0. \tag{17}$$

Then, the right-hand side of Green's formula is brought into

$$-i\langle \phi, \vec{\gamma} \cdot \vec{n}\, \psi \rangle_S = -i\langle \phi_+, \psi_+ \rangle_S + i\langle \phi_-, \psi_- \rangle_S. \tag{18}$$

If the chiral components $\psi_\pm$ of $\psi = \Psi|_S$ are related by

$$\psi_- = U\gamma_{d+1}\psi_+, \tag{19}$$

where U is any unitary operator acting on spinors defined on the boundary and further commutes with $\vec{\gamma} \cdot \vec{n}$, then those components satisfy $\langle \phi_-, \psi_- \rangle_S = \langle \phi_+, \psi_+ \rangle_S$, so that the boundary integral vanishes. The above equation is called the chiral bag boundary condition.

From a physical point of view, we have to consider currents on the boundary. The continuity equation of the current and the density is described as

$$\frac{\partial}{\partial \tau}(\Psi^\dagger \Psi) + \sum_{k=1}^{d} \frac{\partial}{\partial x_k}(\Psi^\dagger \gamma_k \Psi) = 0, \tag{20}$$

where τ denotes the time parameter in this equation only. The transverse component of the current vector $\vec{J} = (\Psi^\dagger \gamma_k \Psi)$, which is given by

$$\Psi^\dagger (\vec{\gamma} \cdot \vec{n}) \Psi, \tag{21}$$

should vanish on the boundary S.

3. Feasible solutions to the 2D Dirac equation

Before solving the Dirac equation for the Hamiltonian $\hat{H}_t$ given in (11), we have to mention the $U(1)$ symmetry of $\hat{H}_t$. Let

$$D(e^{i\tau}) := \begin{pmatrix} e^{-i\tau/2} & 0 \\ 0 & e^{i\tau/2} \end{pmatrix}, \quad R(\tau) := \begin{pmatrix} \cos\tau & -\sin\tau \\ \sin\tau & \cos\tau \end{pmatrix}, \quad \tau \in \mathbb{R}. \tag{22}$$

Then, the $U(1)$ action U_τ on the two-component spinor Φ on $\mathbb{R}^2$ is defined to be

$$U_\tau \Phi = D(e^{i\tau})\Phi \circ R(-\tau). \tag{23}$$

As is straightforwardly verified, the $\hat{H}_t$ admits the $U(1)$ symmetry,

$$U_\tau \hat{H}_t U_\tau^{-1} = \hat{H}_t. \tag{24}$$

The infinitesimal generator $\hat{J}$ of U_τ, which is defined through $U_\tau = \exp(-i\tau\hat{J})$, is called the (spin-orbital) angular momentum operator. By differentiation of U_τ with respect to τ at $\tau = 0$, we obtain

$$\hat{J} = \frac{1}{2}\sigma_3 + i\mathbb{1}\left(q_2\frac{\partial}{\partial q_1} - q_1\frac{\partial}{\partial q_2}\right) = \frac{1}{2}\sigma_3 - i\mathbb{1}\frac{\partial}{\partial \theta}, \tag{25}$$

where (r, θ) are the polar coordinates. The differentiation of (24) with respect to τ at $\tau = 0$ yields

$$[\hat{J}, \hat{H}_t] = 0. \tag{26}$$

The Hamiltonian (11) is expressed in the polar coordinates as

$$\hat{H}_t = -i\sigma_r\frac{\partial}{\partial r} - \frac{i}{r}\sigma_\theta\frac{\partial}{\partial \theta} + t\sigma_3, \tag{27}$$

where
$$\sigma_r = \begin{pmatrix} 0 & e^{-i\theta} \\ e^{i\theta} & 0 \end{pmatrix}, \quad \sigma_\theta = \begin{pmatrix} 0 & -ie^{-i\theta} \\ ie^{i\theta} & 0 \end{pmatrix}. \tag{28}$$

We now apply the separation of variables method in the polar coordinates. We start with the eigenvalue equation $J\Phi = j\Phi$, which is solved by

$$\Phi_j(r,\theta) = \begin{pmatrix} e^{i(j-\frac{1}{2})\theta}\phi_j^{(-)}(r) \\ e^{i(j+\frac{1}{2})\theta}\phi_j^{(+)}(r) \end{pmatrix}, \quad j \in \{\pm\frac{1}{2}, \pm\frac{3}{2}, \cdots\}, \tag{29}$$

where $\phi_j^{(\pm)}(r)$ are unknown radial functions. The Dirac equation $\hat{H}_t\Phi = E\Phi$ then reduces to $\hat{H}_t\Phi_j = E_j\Phi_j$, which gives for radial functions $\phi_j^{(\pm)}(r)$

$$-i\frac{d\phi_j^{(+)}}{dr} - \frac{i}{r}(j + \frac{1}{2})\phi_j^{(+)} + t\phi_j^{(-)} = E_j\phi_j^{(-)}, \tag{30a}$$

$$-i\frac{d\phi_j^{(-)}}{dr} + \frac{i}{r}(j - \frac{1}{2})\phi_j^{(-)} - t\phi_j^{(+)} = E_j\phi_j^{(+)}. \tag{30b}$$

These equations are put together to give rise to a second-order differential equation. According as $|E_j| > |t|$ or $|E_j| < |t|$, the differential equation in question is the Bessel equation or the modified Bessel equation.
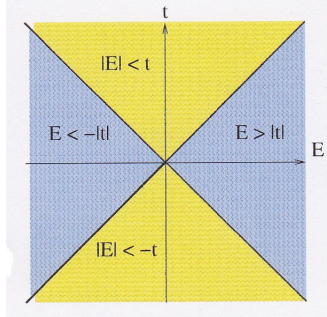

FIGURE 6. The (E, t)-parameter space is divided into four regions with different solutions to (30).

To each of four regions shown in Fig. 6, assigned is a type of feasible solution:

(i) Feasible solutions with $|E_j| > |t|$:

$$\Phi_j(r,\theta) = c\begin{pmatrix} \sqrt{E_j + t}e^{i(j-\frac{1}{2})\theta}J_{j-\frac{1}{2}}(\beta_j r) \\ i\sqrt{E_j - t}e^{i(j+\frac{1}{2})\theta}J_{j+\frac{1}{2}}(\beta_j r) \end{pmatrix} \quad \text{for} \quad E_j > 0, \tag{31a}$$

$$\Phi_j(r,\theta) = c'\begin{pmatrix} \sqrt{|E_j + t|}e^{i(j-\frac{1}{2})\theta}J_{j-\frac{1}{2}}(\beta_j r) \\ -i\sqrt{|E_j - t|}e^{i(j+\frac{1}{2})\theta}J_{j+\frac{1}{2}}(\beta_j r) \end{pmatrix} \quad \text{for} \quad E_j < 0, \tag{31b}$$

where $\beta_j = \sqrt{E_j^2 - t^2}$ and where c and c' are complex constants.

(ii) Feasible solutions with $|E_j| < |t|$:

$$\Phi_j(r, \theta) = c \begin{pmatrix} \sqrt{t + E_j}\, e^{i(j-\frac{1}{2})\theta} I_{j-\frac{1}{2}}(\varepsilon_j r) \\ -i\sqrt{t - E_j}\, e^{i(j+\frac{1}{2})\theta} I_{j+\frac{1}{2}}(\varepsilon_j r) \end{pmatrix} \qquad \text{for} \quad t > 0, \qquad (32a)$$

$$\Phi_j(r, \theta) = c' \begin{pmatrix} \sqrt{|t + E_j|}\, e^{i(j-\frac{1}{2})\theta} I_{j-\frac{1}{2}}(\varepsilon_j r) \\ i\sqrt{|t - E_j|}\, e^{i(j+\frac{1}{2})\theta} I_{j+\frac{1}{2}}(\varepsilon_j r) \end{pmatrix} \qquad \text{for} \quad t < 0, \qquad (32b)$$

where $\varepsilon_j = \sqrt{t^2 - E_j^2}$ and where c and c' are complex constants.

In the limit as $t \to 0$ within the constraint $|E_j| < |t|$, one has $E_j = t = 0$.

(iii) Feasible solutions with $E_j = t = 0$:

$$\Phi_j(r, \theta) = c \begin{pmatrix} 0 \\ e^{i(j+\frac{1}{2})\theta} r^{-(j+\frac{1}{2})} \end{pmatrix} \qquad \text{for} \quad j < 0, \qquad (33a)$$

$$\Phi_j(r, \theta) = c' \begin{pmatrix} e^{i(j-\frac{1}{2})\theta} r^{j-\frac{1}{2}} \\ 0 \end{pmatrix} \qquad \text{for} \quad j > 0. \qquad (33b)$$

In terms of $z = re^{i\theta}$, these solutions are expressed as

$$c \begin{pmatrix} 0 \\ \overline{z}^{|j|-\frac{1}{2}} \end{pmatrix} \quad \text{for} \quad j < 0, \quad \text{and} \quad c' \begin{pmatrix} z^{j-\frac{1}{2}} \\ 0 \end{pmatrix} \quad \text{for} \quad j > 0, \qquad (34)$$

respectively, where $|j| - \frac{1}{2}$ and $j - \frac{1}{2}$ are non-negative integers.

4. The APS boundary condition

Let A_t be the restriction of $\hat{H}_t$ to the circle $r = R$. The boundary operator B_t is then defined to be and expressed as

$$B_t = i\sigma_r A_t = \begin{pmatrix} \frac{i}{R}\frac{\partial}{\partial \theta} & -ite^{-i\theta} \\ ite^{i\theta} & -\frac{i}{R}\frac{\partial}{\partial \theta} \end{pmatrix}, \qquad (35)$$

where $t \neq 0$. The case of $t = 0$ will be treated separately. Further, we note that

$$\sigma_r B_t + B_t \sigma_r = \frac{1}{R}\sigma_r. \qquad (36)$$

Eigenvalues and associated eigenstates of B_t are easily obtained as follows:

$$\phi_j^{(-)}(\theta) = c_j' \begin{pmatrix} -it\, e^{i(j-\frac{1}{2})\theta} \\ (\frac{j}{R} + \lambda_j^-)e^{i(j+\frac{1}{2})\theta} \end{pmatrix} \qquad \text{for} \quad \kappa_j^- := \frac{1}{2R} + \lambda_j^- < 0, \qquad (37a)$$

$$\phi_j^{(+)}(\theta) = c_j \begin{pmatrix} -it\, e^{i(j-\frac{1}{2})\theta} \\ (\frac{j}{R} + \lambda_j^+)e^{i(j+\frac{1}{2})\theta} \end{pmatrix} \qquad \text{for} \quad \kappa_j^+ := \frac{1}{2R} + \lambda_j^+ > 0, \qquad (37b)$$

where

$$\lambda_j^\pm = \pm\sqrt{\frac{j^2}{R^2} + t^2}, \quad t \neq 0. \qquad (38)$$

Let D_R^2 and ∂D_R^2 denote the 2-disk of radius R and its boundary, respectively. Define

$$\mathcal{H}^{(\pm)}(\partial D_R^2) = \mathrm{span}\left\{ \phi_j^{(\pm)}, \, j \in \{\pm\tfrac{1}{2}, \pm\tfrac{2}{3}, \cdots \} \right\}. \qquad (39)$$

Then, the Hilbert space $\mathcal{H}(\partial D_R^2)$ attached to ∂D_R^2 is decomposed into

$$\mathcal{H}(\partial D_R^2) = \mathcal{H}^{(+)}(\partial D_R^2) \oplus \mathcal{H}^{(-)}(\partial D_R^2), \qquad (40)$$

where

$$\mathcal{H}^{(+)}(\partial D_R^2) \perp \mathcal{H}^{(-)}(\partial D_R^2), \quad \sigma_r \mathcal{H}^{(\mp)}(\partial D_R^2) = \mathcal{H}^{(\pm)}(\partial D_R^2). \qquad (41)$$

The APS boundary condition for $t \neq 0$ is now described as

$$\Phi_j(R, \theta) \in \mathcal{H}^{(-)}(\partial D_R^2) \quad \text{or} \quad \Phi_j(R, \theta) \in \mathcal{H}^{(+)}(\partial D_R^2). \qquad (42)$$

In what follows, we list functional equations to determine eigenvalues [6].

(i) Edge state eigenvalues with $\Phi_j(R, \theta) \in \mathcal{H}^{(-)}(\partial D_R^2)$ are determined by the functional equations

$$t\sqrt{\frac{t + E_j}{t - E_j}} I_{j-\frac{1}{2}}(\varepsilon_j R) = \left(\frac{j}{R} + \sqrt{\frac{j^2}{R^2} + t^2} \right) I_{j+\frac{1}{2}}(\varepsilon_j R), \quad \text{for} \quad t > 0, \ (43a)$$

$$|t|\sqrt{\frac{|t + E_j|}{|t - E_j|}} I_{j-\frac{1}{2}}(\varepsilon_j R) = \left(\frac{j}{R} + \sqrt{\frac{j^2}{R^2} + t^2} \right) I_{j+\frac{1}{2}}(\varepsilon_j R), \quad \text{for} \quad t < 0. \ (43b)$$

These equations can be solved numerically to provide edge state eigenvalues as functions of t, as is shown in Fig. 7.
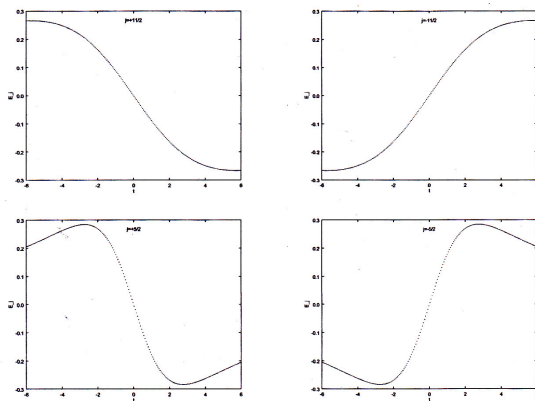

FIGURE 7. Edge state eigenvalues as functions of t. Left panels are for $j = 11/2$, $j = 5/2$, and right panels for $j = -11/2$ and $j = -5/2$.

(ii) There exist no edge state eigenvalues with $\Phi_j(R, \theta) \in \mathcal{H}^{(+)}(\partial D_R^2)$.

(iii) Regular state eigenvalues with $\Phi_j(R,\theta) \in \mathcal{H}^{(-)}(\partial D_R^2)$ are determined by the functional equations

$$-t\sqrt{\frac{E_j + t}{E_j - t}}J_{j-\frac{1}{2}}(\beta_j R) = \left(\frac{j}{R} + \sqrt{\frac{j^2}{R^2} + t^2}\right)J_{j+\frac{1}{2}}(\beta_j R) \quad \text{for} \quad E_j > 0,$$

(44a)

$$t\sqrt{\frac{|E_j + t|}{|E_j - t|}}J_{j-\frac{1}{2}}(\beta_j R) = \left(\frac{j}{R} + \sqrt{\frac{j^2}{R^2} + t^2}\right)J_{j+\frac{1}{2}}(\beta_j R) \quad \text{for} \quad E_j < 0.$$

(44b)

(iv) Regular state eigenvalues with $\Phi_j(R,\theta) \in \mathcal{H}^{(+)}(\partial D_R^2)$ are determined by the functional equations

$$-t\sqrt{\frac{|E_j + t|}{|E_j - t|}}J_{j-\frac{1}{2}}(\beta_j R) = \left(\frac{j}{R} - \sqrt{\frac{j^2}{R^2} + t^2}\right)J_{j+\frac{1}{2}}(\beta_j R) \quad \text{for} \quad E_j > 0,$$

(45a)

$$t\sqrt{\frac{|E_j + t|}{|E_j - t|}}J_{j-\frac{1}{2}}(\beta_j R) = \left(\frac{j}{R} - \sqrt{\frac{j^2}{R^2} + t^2}\right)J_{j+\frac{1}{2}}(\beta_j R) \quad \text{for} \quad E_j < 0.$$

(45b)

Equations (44) and (45) are numerically solved to give regular and edge state eigenvalues as functions of t, respectively, as is shown in Fig. 8.
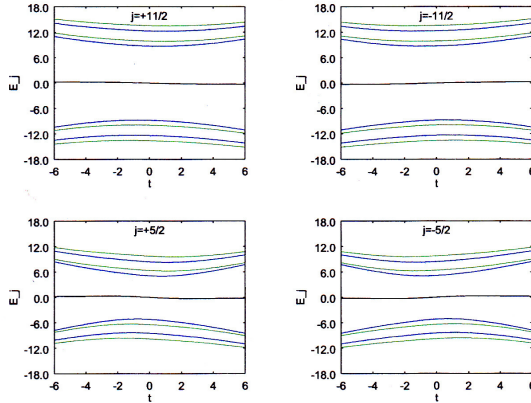

FIGURE 8. Regular state eigenvalues as functions of t under the APS boundary condition. Green lines are eigenvalues with $\Phi_j(R,\theta) \in \mathcal{H}^{(-)}(\partial D_R^2)$. Blue lines are eigenvalues with $\Phi_j(R,\theta) \in \mathcal{H}^{(+)}(\partial D_R^2)$. Black lines are edge state eigenvalues.

We turn to the case of $t = 0$. To pose the APS boundary condition for $t = 0$, we find eigenstates of the boundary operator B_0. From (35) with $t = 0$, the eigenvalues and associated eigenstates for B_0 prove to be given by

$$B_0 \phi_j^{(0,+)} = \frac{1}{R}(j + \frac{1}{2})\phi_j^{(0,+)}, \quad \phi_j^{(0,+)} = \begin{pmatrix} 0 \\ a_j e^{i(j+\frac{1}{2})\theta} \end{pmatrix}, \tag{46a}$$

$$B_0 \phi_j^{(0,-)} = -\frac{1}{R}(j - \frac{1}{2})\phi_j^{(0,-)}, \quad \phi_j^{(0,-)} = \begin{pmatrix} b_j e^{i(j-\frac{1}{2})\theta} \\ 0 \end{pmatrix}. \tag{46b}$$

Now we are in a position to state the APS boundary condition for $t = 0$. Define

$$\mathcal{H}_0^{(\pm)}(\partial D_R^2) = \mathrm{span}\{\phi_j^{(0,\pm)}; \ j = \pm\frac{1}{2}, \pm\frac{3}{2}, \cdots\}. \tag{47}$$

Then, we obtain the decomposition

$$\mathcal{H}(\partial D_R^2) = \mathcal{H}_0^{(+)}(\partial D_R^2) \oplus \mathcal{H}_0^{(-)}(\partial D_R^2), \tag{48}$$

where

$$\mathcal{H}_0^{(+)}(\partial D_R^2) \perp \mathcal{H}_0^{(-)}(\partial D_R^2), \quad \sigma_r \mathcal{H}_0^{(\pm)}(\partial D_R^2) = \mathcal{H}_0^{(\mp)}(\partial D_R^2). \tag{49}$$

In spite of the superscripts ($\pm$), both $\mathcal{H}_0^{(\pm)}(\partial D_R^2)$ have eigenstates associated with negative, zero, and positive eigenvalues of B_0.

The APS boundary condition for $t = 0$ is expressed as

$$\Phi_j(R, \theta) \in \mathcal{H}_0^{(-)}(\partial D_R^2) \quad \text{or} \quad \Phi_j(R, \theta) \in \mathcal{H}_0^{(+)}(\partial D_R^2). \tag{50}$$

The solutions given in (33) are shown to satisfy the APS boundary condition

$$\Phi_j(R, \theta) \in \mathcal{H}_0^{(+)}(\partial D_R^2) \quad \text{for} \quad j < 0, \tag{51a}$$

$$\Phi_j(R, \theta) \in \mathcal{H}_0^{(-)}(\partial D_R^2) \quad \text{for} \quad j > 0. \tag{51b}$$

Eigenstates associated with zero eigenvalue are called zero modes.

We now show that the zero modes are indeed linked with edge eigenstates when the parameter t reaches the zero value. To this end, we introduce the power series $I_\nu^P(z)$ through

$$I_\nu(z) = \left(\frac{z}{2}\right)^\nu I_\nu^P(z), \quad I_\nu^P(z) = \sum_{n=0}^{\infty} \frac{1}{n!\Gamma(\nu + n + 1)} \left(\frac{z}{2}\right)^{2n}. \tag{52}$$

Using $I_{j+\frac{1}{2}}^P(z)$ with $j > 0$ and choosing suitable constant factors, we can modify (32) with prescribed ε_j into the edge eigenstates of the form

$$\tilde{\Phi}_{\mathrm{edg}}^{(+)} = \begin{pmatrix} e^{i(j-\frac{1}{2})\theta} r^{j-\frac{1}{2}} I_{j+\frac{1}{2}}^P(\varepsilon_j r) \\ -i\frac{t - E_j}{2} r^{j+\frac{1}{2}} e^{i(j+\frac{1}{2})\theta} I_{j+\frac{1}{2}}^P(\varepsilon_j r) \end{pmatrix} \quad \text{for} \quad t > 0, \tag{53a}$$

$$\tilde{\Phi}_{\mathrm{edg}}^{(-)} = \begin{pmatrix} e^{i(j-\frac{1}{2})\theta} r^{j-\frac{1}{2}} I_{j+\frac{1}{2}}^P(\varepsilon_j r) \\ i\frac{|t - E_j|}{2} r^{j+\frac{1}{2}} e^{i(j+\frac{1}{2})\theta} I_{j+\frac{1}{2}}^P(\varepsilon_j r) \end{pmatrix} \quad \text{for} \quad t < 0. \tag{53b}$$

Then, as t tends to zero, the both edge states $\tilde{\Phi}_{\text{edg}}^{(\pm)}$ prove to reach the same limit,

$$\tilde{\Phi}_{\text{edg}}^{(-)} \longrightarrow \frac{1}{\Gamma(j+\frac{1}{2})} \begin{pmatrix} r^{j-\frac{1}{2}}e^{i(j-\frac{1}{2})\theta} \\ 0 \end{pmatrix} \longleftarrow \tilde{\Phi}_{\text{edg}}^{(+)}, \quad \text{as} \quad E_j \to 0. \qquad (54)$$

In a similar manner, for the eigenstates defined for $j < 0$ to be

$$\tilde{\Psi}_{\text{edg}}^{(+)} = \begin{pmatrix} \frac{t+E_j}{2}e^{-i(|j|+\frac{1}{2})\theta}r^{|j|+\frac{1}{2}}I_{|j|+\frac{1}{2}}^{P}(\varepsilon_j r) \\ -ie^{-i(|j|-\frac{1}{2})\theta}r^{|j|-\frac{1}{2}}I_{|j|-\frac{1}{2}}^{P}(\varepsilon_j r) \end{pmatrix} \quad \text{for} \quad t > 0, \qquad (55a)$$

$$\tilde{\Psi}_{\text{edg}}^{(-)} = \begin{pmatrix} -\frac{|t+E_j|}{2}e^{-i(|j|+\frac{1}{2})\theta}r^{|j|+\frac{1}{2}}I_{|j|+\frac{1}{2}}^{P}(\varepsilon_j r) \\ -ie^{-i(|j|-\frac{1}{2})\theta}r^{|j|-\frac{1}{2}}I_{|j|-\frac{1}{2}}^{P}(\varepsilon_j r) \end{pmatrix} \quad \text{for} \quad t < 0, \qquad (55b)$$

we find that

$$\tilde{\Psi}_{\text{edg}}^{(-)} \longrightarrow \frac{1}{\Gamma(|j|+\frac{1}{2})} \begin{pmatrix} 0 \\ -ie^{-i(|j|-\frac{1}{2})\theta}r^{|j|-\frac{1}{2}} \end{pmatrix} \longleftarrow \tilde{\Psi}_{\text{edg}}^{(+)}, \quad \text{as} \quad E_j \to 0. \quad (56)$$

　　In the rest of this section, we discuss discrete symmetry and currents on the boundary. As is easily verified, the operators H_t, J, and B_t defining the Dirac equation with the APS boundary condition satisfy

$$\sigma_1 \overline{H}_t \sigma_1 = -H_t, \qquad (57a)$$

$$\sigma_1 \overline{J} \sigma_1 = -J, \qquad (57b)$$

$$\sigma_1 \overline{B}_t \sigma_1 = B_t. \qquad (57c)$$

These equations imply that if E_j is a regular (resp. edge) state eigenvalue with the angular momentum j then $-E_j$ is a regular (resp. edge) state eigenvalue with the angular momentum $-j$. This fact explains the pattern of eigenvalues shown in Figs. 7 and 8. If the graph of one of left panels is reflected with respect to the t-axis (the horizontal axis with $E = 0$), then the resultant graph coincides with the graph of the adjacent right panel.

　　We turn to another discrete symmetry. In a similar manner to the above, we verify that

$$i\sigma_2 \overline{H}_t(-i\sigma_2) = H_{-t}, \qquad (58a)$$

$$i\sigma_2 \overline{J}(-i\sigma_2) = -J, \qquad (58b)$$

$$i\sigma_2 \overline{B}_t(-i\sigma_2) = B_{-t}. \qquad (58c)$$

It then follows that if E_j is a regular (resp. edge) state eigenvalue with the angular momentum j for t, then E_j is a regular (resp. edge) state eigenvalue with the angular momentum $-j$ for $-t$. This fact explains that the pattern of eigenvalues shown in Figs. 7 and 8 is of t-reflection along with j-inversion.

　　We proceed to currents on the boundary. We recall that the boundary values of both edge and regular eigenstates are proportional to eigenstates of the boundary operator B_t. Then, we can easily verify that the radial and the

tangential components of the current for $\phi_j^{(\pm)}$ given in (37) are evaluated as

$$(\phi_j^{(\pm)})^\dagger \sigma_r \phi_j^{(\pm)} = 0, \quad (\phi_j^{(\pm)})^\dagger \sigma_\theta \phi_j^{(\pm)} = 2t|c|^2 \left(\frac{j}{R} \pm \sqrt{\frac{j^2}{R^2} + t^2} \right), \qquad (59)$$

respectively, where c is a constant. While the radial component vanishes, the tangential component alternates the sign, according as $t < 0$ or $t > 0$.

5. The chiral bag boundary condition

If the unitary operator U in (19) is chosen as

$$U = e^{2i \arctan e^\lambda} \mathbb{1}, \qquad (60)$$

the chiral bag boundary condition is brought into

$$\sigma_r \psi = -ie^{\lambda \sigma_3} \sigma_3 \psi. \qquad (61)$$

With this boundary condition applied to feasible solutions, the functional equations for determining edge and regular state eigenvalues are found to be given as follows [7]: (i) For $|E_j| < |t|$, those functional equations are

$$\sqrt{\frac{t + E_j}{t - E_j}} I_{j-\frac{1}{2}}(\varepsilon_j R) = e^{-\lambda} I_{j+\frac{1}{2}}(\varepsilon_j R) \quad \text{for} \quad t > 0, \qquad (62a)$$

$$-\sqrt{\frac{|t + E_j|}{|t - E_j|}} I_{j-\frac{1}{2}}(\varepsilon_j R) = e^{-\lambda} I_{j+\frac{1}{2}}(\varepsilon_j R) \quad \text{for} \quad t < 0, \qquad (62b)$$

and (ii) for $|E_j| > |t|$, they are

$$\sqrt{\frac{E_j + t}{E_j - t}} J_{j-\frac{1}{2}}(\beta_j R) = -e^{-\lambda} J_{j+\frac{1}{2}}(\beta_j R) \quad \text{for} \quad E_j > 0, \qquad (63a)$$

$$\sqrt{\frac{|E_j + t|}{|E_j - t|}} J_{j-\frac{1}{2}}(\beta R) = e^{-\lambda} J_{j+\frac{1}{2}}(\beta_j R) \quad \text{for} \quad E_j < 0. \qquad (63b)$$

Though Eq. (62b) has no solution, the other functional equations for regular and edge state eigenvalues are numerically solved to provide the eigenvalues as functions of t, as is shown in Fig. 9.

A remarkable property observed in Fig. 9 is that one of regular state eigenvalues is connected with an edge state eigenvalue. We refer to the state as a critical state, which corresponds to the eigenvalue as a limit of both the regular and the edge state eigenvalues. Since the critical states are characterized by the conditions that $E = \pm t$, we can easily solve Eq. (30) with $E = \pm t$ to find the critical states within constant multiples, along with the
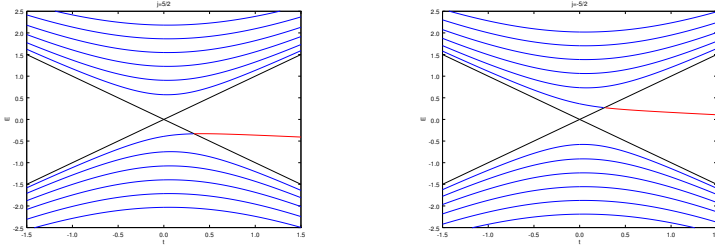
FIGURE 9. Eigenvalues of regular (blue) and edge (red) eigenstates with $R = 10, \lambda = 0.1$ for $j = 5/2$ (left panel) and for $j = -5/2$ (right panel).

eigenvalues,

$$\Phi = \begin{pmatrix} ir^{j-\frac{1}{2}}e^{i(j-\frac{1}{2})\theta} \\ \frac{e^{\lambda}}{R}r^{j+\frac{1}{2}}e^{i(j+\frac{1}{2})\theta} \end{pmatrix}, \quad E_j^{\mathrm{cri}} = -\frac{e^{\lambda}(j+\frac{1}{2})}{R}, \text{ for } j > 0, \tag{64a}$$

$$\Phi = \begin{pmatrix} -\frac{e^{-\lambda}}{R}r^{-(j-\frac{1}{2})}e^{i(j-\frac{1}{2})\theta} \\ ir^{-(j+\frac{1}{2})}e^{i(j+\frac{1}{2})\theta} \end{pmatrix}, \quad E_j^{\mathrm{cri}} = \frac{e^{-\lambda}(|j|+\frac{1}{2})}{R}, \text{ for } j < 0. \tag{64b}$$

Like (34), these critical states are also described in $z = re^{i\theta}$ as

$$\Phi = \begin{pmatrix} iz^{j-\frac{1}{2}} \\ \frac{e^{\lambda}}{R}z^{j+\frac{1}{2}} \end{pmatrix}, \quad j > 0, \tag{65a}$$

$$\Phi = \begin{pmatrix} -\frac{e^{-\lambda}}{R}\overline{z}^{|j|+\frac{1}{2}} \\ i\overline{z}^{|j|-\frac{1}{2}} \end{pmatrix}, \quad j < 0. \tag{65b}$$

We can verify that the transition indeed occurs from a regular eigenstate to an edge eigenstate. Like (53), choosing a suitable scaling factor, we can introduce a regular and an edge eigenstates for $j > 0$ of the form

$$\tilde{\Phi}_{\mathrm{reg}} = \begin{pmatrix} r^{j-\frac{1}{2}}e^{i(j-\frac{1}{2})\theta}J_{j-\frac{1}{2}}^P(\beta_j r) \\ -i\frac{|E_j-t|}{2}r^{j+\frac{1}{2}}e^{i(j+\frac{1}{2})\theta}J_{j+\frac{1}{2}}^P(\beta_j r) \end{pmatrix}, \tag{66a}$$

$$\tilde{\Phi}_{\mathrm{edg}} = \begin{pmatrix} e^{i(j-\frac{1}{2})\theta}r^{j-\frac{1}{2}}I_{j+\frac{1}{2}}^P(\varepsilon_j r) \\ -i\frac{t-E_j}{2}r^{j+\frac{1}{2}}e^{i(j+\frac{1}{2})\theta}I_{j+\frac{1}{2}}^P(\varepsilon_j r) \end{pmatrix}, \tag{66b}$$

respectively, where J_ν^P is a power series defined through

$$J_\nu(z) = \left(\frac{z}{2}\right)^\nu J_\nu^P(z), \quad J_\nu^P(z) = \sum_{n=0}^{\infty} \frac{(-1)^n}{n!\Gamma(\nu+n+1)}\left(\frac{z}{2}\right)^{2n}. \tag{67}$$

It is easily shown that as $E_j(t) \to -t$, there occurs the transition

$$\tilde{\Phi}_{\mathrm{reg}} \longrightarrow \frac{1}{\Gamma(j+\frac{1}{2})}\begin{pmatrix} r^{j-\frac{1}{2}}e^{i(j-\frac{1}{2})\theta} \\ -i\frac{e^{\lambda}}{R}r^{j+\frac{1}{2}}e^{i(j+\frac{1}{2})\theta} \end{pmatrix} \longleftarrow \tilde{\Phi}_{\mathrm{edg}}. \tag{68}$$

For $j < 0$, we take

$$\tilde{\Psi}_{\text{reg}} = \begin{pmatrix} \frac{E_j + t}{2} e^{-i(|j| + \frac{1}{2})\theta} r^{|j| + \frac{1}{2}} J^P_{|j| + \frac{1}{2}}(\beta_j r) \\ -i e^{-i(|j| - \frac{1}{2})\theta} r^{|j| - \frac{1}{2}} J^P_{|j| - \frac{1}{2}}(\beta_j r) \end{pmatrix}, \tag{69a}$$

$$\tilde{\Psi}_{\text{egd}} = \begin{pmatrix} \frac{t + E_j}{2} e^{-i(|j| + \frac{1}{2})\theta} r^{|j| + \frac{1}{2}} I^P_{|j| + \frac{1}{2}}(\varepsilon_j r) \\ -i e^{-i(|j| - \frac{1}{2})\theta} r^{|j| - \frac{1}{2}} I^P_{|j| - \frac{1}{2}}(\varepsilon_j r) \end{pmatrix}. \tag{69b}$$

Then, a straightforward calculation shows that as $E_j(t) \to t$, there occurs the transition

$$\tilde{\Psi}_{\text{reg}} \longrightarrow \frac{1}{\Gamma(|j| + \frac{1}{2})} \begin{pmatrix} \frac{e^{-\lambda}}{R} e^{-i(|j| + \frac{1}{2})\theta} r^{|j| + \frac{1}{2}} \\ -i e^{-i(|j| - \frac{1}{2})\theta} r^{|j| - \frac{1}{2}} \end{pmatrix} \longleftarrow \tilde{\Psi}_{\text{edg}}. \tag{70}$$

In the rest of this section, we mention discrete symmetry and boundary currents. Like (57), we verify that

$$\sigma_1 \overline{H}_t \sigma_1 = -H_t, \tag{71a}$$

$$\sigma_1 \overline{J} \sigma_1 = -J, \tag{71b}$$

$$\sigma_r \sigma_1 \overline{\psi} = -i e^{-\lambda \sigma_3} \sigma_3 \sigma_1 \overline{\psi}. \tag{71c}$$

In contrast to (57c), the chiral bag boundary condition is not invariant under the $\sigma_1 K$, where K denotes the complex conjugation. In fact, in the right-hand side of (71c), the exponent λ of the boundary condition (61) is replaced by $-\lambda$. However, if the λ is viewed as a real parameter, the inversion $\lambda \to -\lambda$ is acceptable as a transformation, so that we may view the above equations as representing a pseudo-symmetry of the family of the Dirac equations with the chiral bag boundary condition depending on λ. It then turns out that if E_j is a regular (resp. edge) state eigenvalue with the angular momentum j then $-E_j$ is a regular (resp. edge) state eigenvalue with the angular momentum $-j$ under the boundary condition with the parameter value $-\lambda$. This symmetry is observed in the pattern of eigenvalues shown in Fig.10.
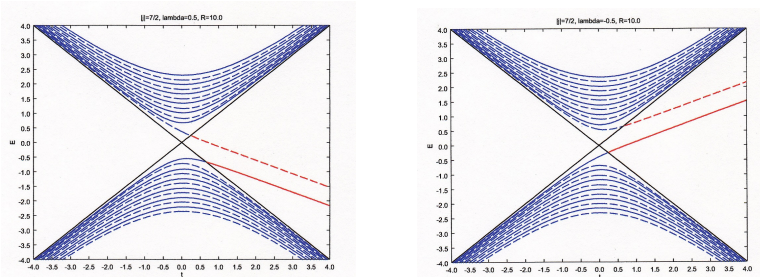

FIGURE 10. Eigenvalues of regular (blue) and edge (red) eigenstates with $|j| = \frac{7}{2}$, $R = 10$ and with $\lambda = -0.5$ (left panel) and $\lambda = 0.5$ (right panel). The solid and dashed curves are for $j > 0$ and for $j < 0$, respectively. Black lines are auxiliary lines $E = \pm t$ separating the regions referred to in Fig. 6.

In contrast to (58), the operator $i\sigma_2 K$ cannot be a symmetry operator for the eigenvalue problem with the chiral bag boundary condition. In fact, we obtain the following equations in correspondence with (58),

$$i\sigma_2 \overline{H}_t(-i\sigma_2) = H_{-t}, \tag{72a}$$

$$i\sigma_2 \overline{J}(-i\sigma_2) = -J, \tag{72b}$$

$$\sigma_r(i\sigma_2)\overline{\psi} = ie^{-\lambda\sigma_3}\sigma_3(i\sigma_2)\overline{\psi}. \tag{72c}$$

As is seen in (72c), the boundary condition is not (pseudo-)invariant under the action of $i\sigma_2 K$. In the right-hand side of the (72c), the factor $-i$ of the condition (61) is replaced by i. This gives a reason why the pattern of eigenvalues shown in Fig. 10 is not of t-reflection along with j-inversion.

Currents on the boundary for edge states (32) with $r = R$ and E_j specified are given, within constant multiples, by

$$\psi^\dagger \sigma_r \psi = 0, \tag{73a}$$

$$\psi^\dagger \sigma_\theta \psi = -2(t + E_j)e^\lambda I_{j-\frac{1}{2}}(\varepsilon_j R)^2 \quad \text{for} \quad t > 0. \tag{73b}$$

For regular states (31) with $r = R$ and E_j specified, one has, within constant multiples,

$$\psi^\dagger \sigma_r \psi = 0, \tag{74a}$$

$$\psi^\dagger \sigma_\theta \psi = \begin{cases} -2(t + E_j)e^\lambda J_{j-\frac{1}{2}}(\beta_j R)^2 & \text{for} \quad E_j > 0, \\ -2|t + E_j|e^\lambda J_{j-\frac{1}{2}}(\beta_j R)^2 & \text{for} \quad E_j < 0. \end{cases} \tag{74b}$$

6. Comparison between the APS and the chiral bag boundary conditions

We are interested in transition states both for the APS and the chiral bag boundary conditions. As is well known, the spectral flow for a one-parameter
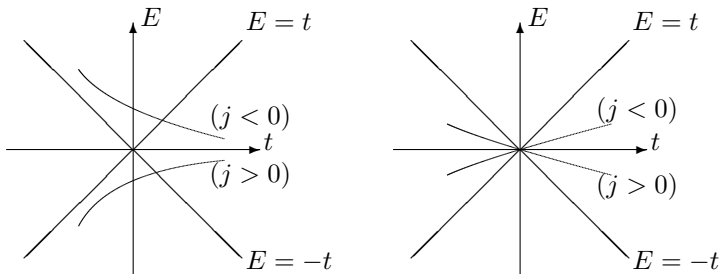

FIGURE 11. A schematic view of transient eigenvalue curves. The left and the right panels are for the chiral bag and the APS boundary conditions, respectively. In the left panel, the parameter is chosen as $\lambda = 0$ for simplicity.

family of operators is the net number of eigenvalues passing through zero

in the positive direction as the parameter runs. This notion works well for characterizing the band rearrangement under the APS boundary condition. In fact, the spectral flow in question is given by $-\text{sgn}(j)$. However, it does not serve as a characteristic quantity under the chiral bag boundary condition, since the zero eigenvalue does not carry a special meaning.
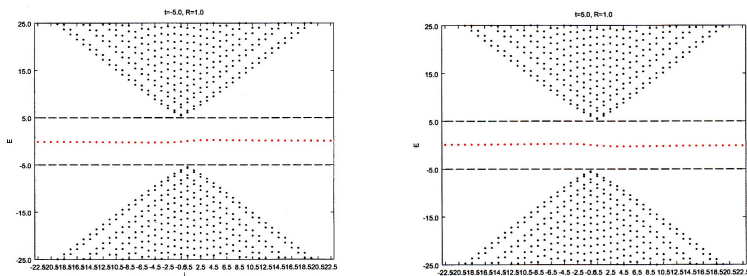

FIGURE 12. Eigenvalues of regular (black) and edge (red) eigenstates against j under the APS boundary condition with $R = 1.0$ for $t = -5.0$ (left panel) and for $t = 5.0$ (right panel). The dashed horizontal lines in the left and the right panels correspond to the lines $E = \pm t$ with $t = -5.0$ and $t = 5.0$, respectively.
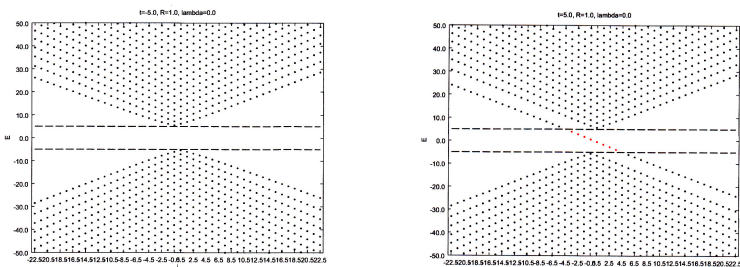

FIGURE 13. Eigenvalues of regular (black) and edge (red) eigenstates against j under the chiral bag boundary condition with $R = 1.0, \lambda = 0.0$ for $t = -5.0$ (left panel) and for $t = 5.0$ (right panel). The dashed horizontal lines in the left and the right panels correspond to the lines $E = \pm t$ with $t = -5.0$ and $t = 5.0$, respectively.

We need an extended notion of the spectral flow to characterize the band rearrangement under the chiral bag boundary condition. In the case of the chiral bag boundary condition, there exists a transient eigenvalue curve which crosses one of the boundary lines $E = \pm t$, depending on whether $j > 0$ or $j < 0$ (see Fig. 11, the left and the right panels of which are abstracted from Fig. 9 and Fig. 7, respectively). If we assign -1 and $+1$ to the crossing of the boundary lines $E = -t$ and $E = t$, respectively, the extended spectral

flow for the chiral bag boundary condition is given by $-\text{sgn}(j)$. Then, band rearrangement is characterized by $-\text{sgn}(j)$ in both cases of the APS and the chiral bag boundary conditions.

In conclusion, we compare two boundary conditions from another point of view. If we plot energy eigenvalues against j under the chiral bag boundary condition with the parameter t fixed at a value, we obtain Figs. 12 and 13 for the APS and the chiral bag boundary conditions, respectively. Difference is distinctively observed in the pattern of edge state eigenvalues (red dots).

Acknowledgment

References

[1] M. Asorey, A.P. Balachandran, and J.M. Pérez-Pardo, *Edge states: topological insulators, superconductors and QCD chiral bags*, JHEP (12)073 (2013).

[2] F. Faure and B. Zhilinskii, *Topological Chern indices in molecular spectra*, Phys. Rev. Lett. vol.**85**, 960-963 (2000).

[3] T. Iwai and B. Zhilinskii, *Energy bands: Chern numbers and symmetry*, Ann. Phys., vol.**326**, 3013-3066 (2011).

[4] T. Iwai and B. Zhilinskii, *Rearrangement of energy bands: Chern numbers in the presence of cubic symmetry*, Acta Appl. Math., vol.**120**, 153-175 (2012).

[5] T. Iwai and B. Zhilinskii, *Qualitative features of the rearrangement of molecular energy spectra from a "wall-crossing" perspective*, Phys. Lett. A**377**, 2481-2486 (2013).

[6] T. Iwai and B. Zhilinskii, *Local description of band rearrangements; comparison of semi-quantum and full quantum approach*, Acta Appl. Math. **137**, 97-121 (2015).

[7] T. Iwai and B. Zhilinskii, *Band rearrangement through the 2D-Dirac equations with boundary conditions*, submitted.

Toshihiro Iwai
Kyoto University
Kyoto, Japan
e-mail: `iwai.toshihiro.63u@st.kyoto-u.ac.jp`

Boris Zhilinskii
Université du Littoral Côte d'Opale
Dunkerque, France
e-mail: `zhilin@univ-littoral.fr`